COMMUNICATION
Aitian Chen, Xi-Xiang Zhang *et al.*
Giant magnetoelectric effect in perpendicularly magnetized
Pt/Co/Ta ultrathin films on a ferroelectric substrate

ROYAL SOCIETY OF CHEMISTRY

Check for updates

Giant magnetoelectric effect in perpendicularly magnetized Pt/Co/Ta ultrathin films on a ferroelectric substrate†

Aitian Chen, (ID) ∗[a] Haoliang Huang, (ID) [b] Yan Wen,[a] Wenyi Liu,[b] Senfu Zhang,[a] Jürgen Kosel,[c] Weideng Sun,[d] Yonggang Zhao,[d] Yalin Lu[b] and Xi-Xiang Zhang (ID) ∗[a]

Perpendicularly magnetized layers are essential for information storage to increase the storage density. Modulating perpendicular magnetization by an electric field offers a promising solution to lower energy consumption. Here, we demonstrate a remarkable electric field modulation of perpendicular magnetization in perpendicularly magnetized Pt/Co/Ta ultrathin films on a ferroelectric substrate. By measuring the anomalous Hall effect under *in situ* electric fields, we observe a giant magnetoelectric effect with the large converse magnetoelectric coefficient of -2.1×10^{-6} s m^{-1} at $H_\perp = -20$ Oe and -0.9×10^{-6} s m^{-1} at $H_\perp = 0$ Oe, which is comparable to that in multiferroic heterostructures with in-plane magnetization. Additionally, Kerr imaging shows that electric fields observably affect magnetic domain structures of the Pt/Co/Ta ultrathin films indicating a giant magnetoelectric effect. We further measure *in situ* X-ray diffraction and X-ray reflectivity with electric fields, which suggests that this giant magnetoelectric effect is attributed to strain-mediated magnetoelectric coupling and is closely related to electric-field-varied interface roughness. Our findings highlight the role of interface roughness in exploring electrical control of perpendicular magnetization.

New concepts

Perpendicularly magnetized layers are important for increasing the information storage density in perpendicular magnetic recording media, and electric-field control of perpendicular magnetization is drawing much attraction due to its potential to lower energy consumption. Different from previous literature reports on multiferroic heterostructures with perpendicularly magnetized multilayers, here, we deposit perpendicularly magnetized Pt/Co/Ta ultrathin films with a single magnetic layer on a ferroelectric substrate. We obtain a giant magnetoelectric effect with a large converse magnetoelectric coefficient of -2.1×10^{-6} s m^{-1} at $H_\perp = -20$ Oe and -0.9×10^{-6} s m^{-1} at $H_\perp = 0$ Oe, which is the largest in the multiferroic heterostructures with perpendicular magnetization and is also comparable with the largest value in the multiferroic heterostructures with in-plane magnetization. Additionally, owing to only two interfaces Pt/Co and Co/Ta contributing to interface perpendicular magnetic anisotropy in Pt/Co/Ta ultrathin films, we can investigate how an electric field affects the interface perpendicular magnetic anisotropy by measuring *in situ* X-ray reflectivity with electric fields. These results reveal the important role of electric-field-varied interface roughness in modulating PMA in multiferroic heterostructures, which has not been considered before. This work is significant for electric field control of perpendicular magnetization and promising for energy-efficient spintronic devices.

Introduction

Perpendicularly magnetized layers are crucial for developing high density information storage, as it enables shrinking the

[a] Physical Science and Engineering Division, King Abdullah University of Science and Technology, Thuwal 23955-6900, Saudi Arabia.
E-mail: xixiang.zhang@kaust.edu.sa, aitian.chen@kaust.edu.sa

[b] Anhui Laboratory of Advanced Photon Science and Technology, Hefei National Laboratory for Physical Sciences at the Microscale, University of Science and Technology of China, Hefei 230026, China

[c] Computer, Electrical and Mathematical Sciences and Engineering Division, King Abdullah University of Science and Technology, Thuwal 23955-6900, Saudi Arabia

[d] Department of Physics and State Key Laboratory of Low-Dimensional Quantum Physics, Tsinghua University, Beijing 100084, China

† Electronic supplementary information (ESI) available. See DOI: 10.1039/d0mh00796j

size of elements and maintaining thermally stable magnetization states.[1] To write and erase information of the spintronic devices, conventionally, an electric current is injected to control the perpendicularly magnetized layer *via* spin-transfer torque[2] or spin–orbit torque,[3–5] where a large current density larger than a threshold is required. Recently, much effort has been devoted to seeking energy-efficient methods to modulate perpendicular magnetic anisotropy (PMA) in a perpendicularly magnetized layer.[6–8] One of the promising methods is to use electric-field-induced piezostrain in a ferroelectric instead of an electric current. Over the past decade, researchers have been integrating ferroelectric substrates and magnetic materials with in-plane magnetization to form multiferroic heterostructures, and have demonstrated that the in-plane magnetization can be efficiently manipulated by an electric field *via* strain-mediated magnetoelectric coupling,[9–13] which employs the

electric-field-generated piezostrain in the ferroelectric substrate to modulate the magnetic property of the magnetic materials *via* a converse magnetostriction effect. Inspired by this success, several groups have explored the electric-field modulation of perpendicular magnetization by depositing perpendicularly magnetized layers on ferroelectric substrates.[14–22] For instance, Sun *et al.*[14] and Peng *et al.*[15] fabricated Co/Pt multilayers on a Pb(Mg$_{1/3}$Nb$_{2/3}$)$_{0.7}$Ti$_{0.3}$O$_3$ (PMN-PT) ferroelectric substrate and used ferromagnetic resonance (FMR) to investigate the effect of an electric field on their interface PMA. Although the interface PMA was modulated by the electric field through strain-mediated magnetoelectric coupling, the modulation was found not to be remarkable with a small converse magnetoelectric coefficient. Moreover, only the sample around the spin reorientation transition had a magnetoelectric effect.[14,15] Previous work primarily focused on perpendicularly magnetized multilayers with an interface PMA, such as Co/Pt multilayers,[14,15,21] Cu/Ni multilayers[19] and Co/Ni multilayers.[22] In perpendicularly magnetized multilayers, there are several interfaces contributing to the interface PMA, making it complex to analyze the effect of the electric field on each interface. Thus, previous literature reports on multiferroic heterostructures with perpendicular magnetization[14–17,19,21,22] have not taken into account variation of interface roughness induced by electric fields, even though it plays an important role in interface PMA.[23–25] Conversely, only two interfaces, Pt/Co and Co/Ta, contribute to the interface PMA in perpendicularly magnetized Pt/Co/Ta ultrathin films with a single magnetic layer, which provides a pure and simple model to investigate how electric field affects interface PMA. Additionally, the interface PMA of Pt/Co/Ta is sensitive to the roughness of the interface,[23] therefore a remarkable modulation of the interface PMA is expected by electric-field-controlled morphology.[26] However, perpendicularly magnetized Pt/Co/Ta ultrathin films deposited on ferroelectrics have so far not been studied.

Here, we report a giant magnetoelectric effect in perpendicularly magnetized Pt/Co/Ta ultrathin films on a PMN-PT ferroelectric substrate. By measuring the anomalous Hall effect (AHE), we found that electric fields dramatically affected the AHE curves of Pt/Co/Ta, so we achieved a giant magnetoelectric effect whose large converse magnetoelectric coefficient is -2.1×10^{-6} s m^{-1} at $H_\perp = -20$ Oe and -0.9×10^{-6} s m^{-1} at $H_\perp = 0$ Oe. Magnetic domain structures of Pt/Co/Ta ultrathin films also exhibited a remarkable change by applying electric fields, as revealed by Kerr imaging, suggesting a giant magnetoelectric effect. We further measured *in situ* X-ray diffraction (XRD) and X-ray reflectivity (XRR) with electric fields to investigate the electric-field-induced piezostrain and the interface roughness variation of the Pt/Co/Ta ultrathin films. The XRD and XRR results show that this giant magnetoelectric effect originates from the strain-mediated magnetoelectric coupling *via* electric-field-induced interface roughening. These results are significant for electric field control of perpendicular magnetization and promising for energy-efficient spintronic devices.

Results and discussion

Pt/Co/Ta ultrathin films consisting of Ta (3 nm)/Pt (3 nm)/Co (t nm)/Ta (2 nm) multilayers with different Co thicknesses were sputtered on PMN-PT (011) ferroelectric substrates, and a Hall bar shape was patterned by a shadow mask to perform AHE measurements as shown in Fig. S1a (ESI†). The PMN-PT ferroelectric substrates were chosen because of their large piezoelectric coefficient, and have been widely used as the piezoelectric substrate in multiferroic heterostructures[10,14–16,20,21] to produce distinct and stable strain. It is well known that the AHE curve can reflect the out-of-plane magnetic hysteresis loop due to the linear relationship between Hall resistance and perpendicular magnetization, *i.e.*, $R_H \propto M_Z$ (Experimental section). Thus, we first measured the AHE curves of the samples with various thicknesses of Co layer and the results are presented in Fig. S1b (ESI†). The AHE curves for $t = 1.8$ nm and 1.85 nm had a nearly square shape and a sharp switching around the coercive field (H_C), suggesting a strong PMA. As the Co layer thickness increased, the AHE curve became gradual, with a decrease in the normalized R_H value (*i.e.*, $\frac{R_H}{R_{H,S}}$) at zero magnetic field and an increase in the saturated field (H_S), which indicates a reduction in PMA. Applying an electric field to the PMN-PT substrate can generate a piezostrain *via* the converse piezoelectric effect to modulate perpendicular magnetization of Pt/Co/Ta ultrathin films. Next, we investigated how an electric field affects the PMA of Pt/Co/Ta ultrathin films by measuring AHE *in situ* with electric fields, and the results of the samples with various thicknesses of Co layer are shown in Fig. S2 (ESI†). Interestingly, the AHE curves for all the samples exhibited a remarkable change when electric fields were applied. These results are different from previous results regarding Co/Pt multilayers on PMN-PT,[14,15] in which the electrical modulation of PMA was primarily observed in the sample near the spin reorientation transition limited to a small window of Co thickness. For the sample with $t = 1.85$ nm, $\frac{R_H}{R_{H,S}}$ at $H_\perp = 0$ Oe exhibited a remarkable change with the application of electric fields, indicating that M_Z can be tuned by electric fields at zero magnetic field since the remnant $\frac{R_H}{R_{H,S}}$ is proportional to the remnant M_Z. Thus, we primarily investigated the sample with $t = 1.85$ nm in this work.

In situ AHE curves under electric fields for the perpendicularly magnetized Pt/Co/Ta sample with $t = 1.85$ nm are presented in Fig. 1a. The AHE curve under $E = 0$ kV cm^{-1} was square with a sharp switching, and the remnant $\frac{R_H}{R_{H,S}}$ at $H_\perp = 0$ Oe was almost 100%. When applying electric fields, the AHE curves exhibited a distinct change with a reduced squareness. It is evident that the H_C was decreasing and the H_S was increasing with increasing electric fields. These results suggest that an electric field weakens the PMA. We defined the electric field modulation of $\frac{R_H}{R_{H,S}}$, which is proportional to M_Z, as
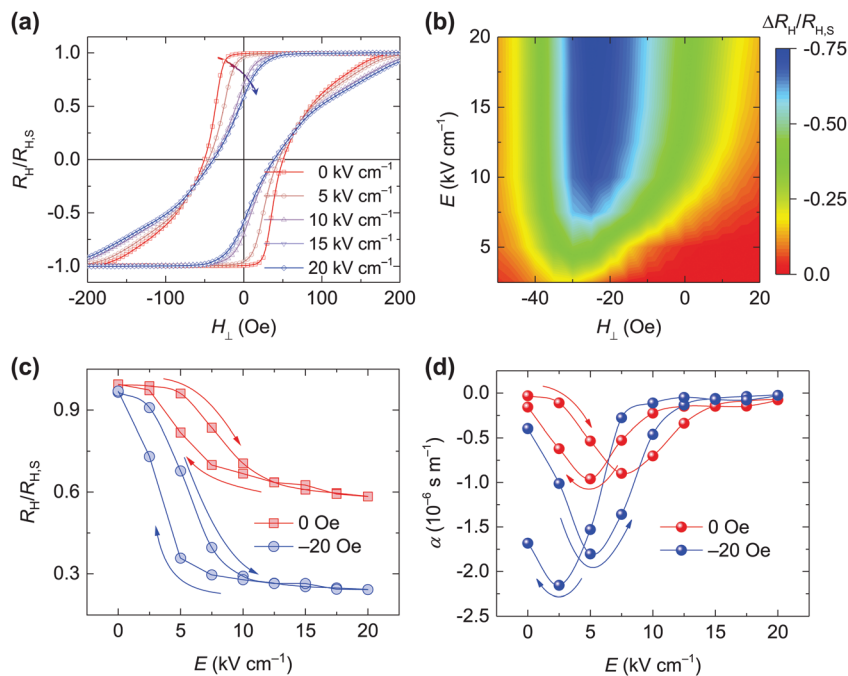
Fig. 1 (a) *In situ* AHE curves measured with electric fields for the perpendicularly magnetized Pt/Co/Ta sample with a 1.85 nm thickness of Co layer. $\frac{R_H}{R_{H,S}}$ decreased as the electric field increased, as shown by the arrow. (b) $\Delta\frac{R_H}{R_{H,S}}$ diagram as a function of $H_\perp$ and electric field deduced from (a). A large electric field modulation of $\frac{R_H}{R_{H,S}}$ was achieved for $H_\perp$ in the range of −40 Oe to 15 Oe. (c) Electric field dependence of $\frac{R_H}{R_{H,S}}$ at $H_\perp$ = 0 Oe and −20 Oe, where a dramatic change occurred between 5 kV cm^{-1} and 10 kV cm^{-1}. (d) Converse magnetoelectric coefficient α at $H_\perp$ = −20 Oe and 0 Oe deduced from (c).

$\Delta\frac{R_H}{R_{H,S}} = \frac{R_H}{R_{H,S}}(E) - \frac{R_H}{R_{H,S}}(0)$, where $\frac{R_H}{R_{H,S}}(E)$ and $\frac{R_H}{R_{H,S}}(0)$ are the normalized Hall resistance with and without electric field, respectively. Fig. 1b presents the diagram of $H_\perp$ and the electric field for $\Delta\frac{R_H}{R_{H,S}}$ deduced from the AHE curves in Fig. 1a. The electric field can effectively modulate $\frac{R_H}{R_{H,S}}$ for $H_\perp$ in the range of −40 Oe to 15 Oe, and the largest modulation with a 0.72 change was observed around −20 Oe. Most importantly, an electric field modulation of $\frac{R_H}{R_{H,S}}$ with a 0.41 change was realized at zero magnetic field, as shown in Fig. 1c, which corresponds to a 41% change in M_Z. Note that the decrease in M_Z under electric fields suggests a decrease of interface PMA in Pt/Co/Ta ultrathin films. These remarkable changes in $\frac{R_H}{R_{H,S}}$ caused by electric fields indicated that the electric fields had an arresting effect on M_Z *via* magnetoelectric coupling, so that M_Z was modulated by electric fields in perpendicularly magnetized Pt/Co/Ta ultrathin films even at zero magnetic field. Fig. 1d shows the converse magnetoelectric coefficient $\alpha = \mu_0\frac{dM_Z}{dE} = \mu_0 M_S\frac{d(R_H/R_{H,S})}{dE}$ (Experimental section) for $H_\perp$ = −20 Oe and 0 Oe, which were deduced from Fig. 1c. It can be found that a peak α of approximately −2.1 × 10^{-6} s m^{-1} was obtained at $H_\perp$ = −20 Oe and a peak α of approximately −0.9 × 10^{-6} s m^{-1}

was obtained at $H_\perp$ = 0 Oe, which indicates a giant magnetoelectric effect in the PMN-PT/Pt/Co/Ta multiferroic heterostructure. To the best of our knowledge, this value of α is the largest in the multiferroic heterostructures with out-of-plane magnetization and is also comparable with the largest value in the multiferroic heterostructures with in-plane magnetization[27,28] (a magnitude of 10^{-6} s m^{-1}).

To gain further insight into this giant magnetoelectric effect in the PMN-PT/Pt/Co/Ta multiferroic heterostructure, polar Kerr imaging was performed to investigate the evolution of magnetic domains under electric fields, as shown in Fig. 2a. The polar Kerr image only displays the magnetic domain of the Pt/Co/Ta ultrathin film and is not sensitive to the ferroelectric domain of the PMN-PT substrate. For each electric field, the Pt/Co/Ta film was first saturated by applying a negative magnetic field of −200 Oe. Then, the Kerr images were acquired at $H_\perp$ = 0 Oe after applying a series of positive magnetic field pulses at a duration of 0.1 s. The magnetic field pulses were applied to reverse magnetization so that the upward magnetic domain appeared and expanded. Note that no cracks caused by electric fields[26] occurred during the measurement for our sample (Fig. 2a). For E = 0 kV cm^{-1}, almost all the magnetic domains reversed after the application of a magnetic field pulse of 80 Oe. As the applied electric fields increased, it became evident that the magnetic field pulses required to fully reverse the magnetic domains were notably decreasing. Moreover, for a certain magnetic field below 60 Oe, the Kerr image primarily had downward domains with a white contrast at E = 0 kV cm^{-1},
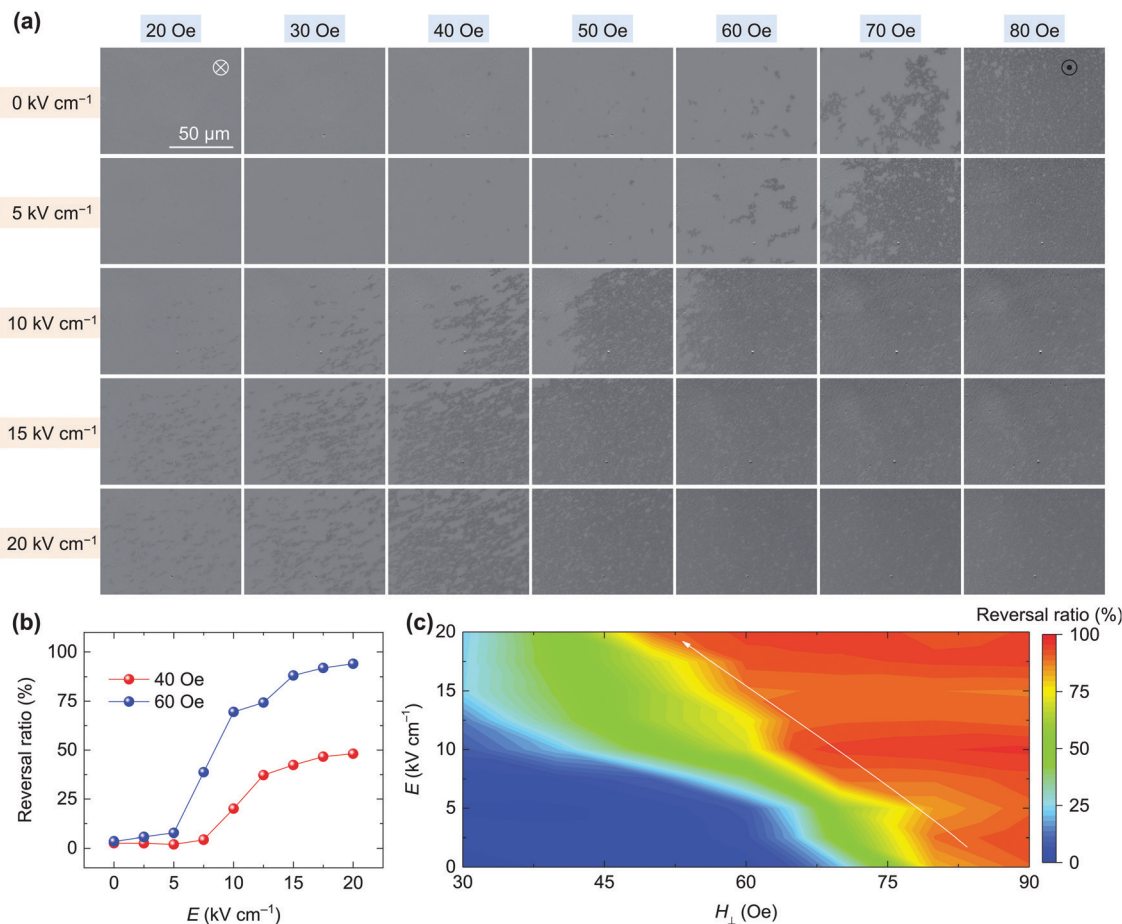
Fig. 2 (a) Magnetic domain structures imaged at various electric fields, after applying sequential magnetic field pulses. Prior to applying positive magnetic field pulses for each electric field, a negative magnetic field of −200 Oe was used to saturate the sample. (b) Magnetic domain reversal ratio as a function of electric field, after applying 40 Oe and 60 Oe. (c) Magnetic domain reversal ratio diagram as a function of the magnetic field and the electric field. The magnetic field pulse required to fully reverse the magnetic domain decreased with increasing electric fields, as shown by the arrow.

and upward domains with a black contrast generated and expanded with increasing electric fields. We further quantified the magnetic domain reversal ratio by statistically analysing the ratio of the upward magnetic domains in each Kerr image of Fig. 2a. For instance, Fig. 2b displays the electric field dependence of the reversal ratio at 40 Oe and 60 Oe magnetic field pulses, at which the reversal ratio increased with increasing electric fields. The differences in the reversal ratio between $E = 0$ kV cm^{-1} and 20 kV cm^{-1} were large: approximately 50% for 40 Oe and approximately 100% for 60 Oe. This indicated a striking effect of the electric field on the domain structure *via* magnetoelectric effect. Furthermore, a diagram of the magnetic field pulse and electric field of the magnetic domain reversal ratio is plotted in Fig. 2c. As shown by the arrow, the amplitude of the magnetic field pulse required to fully reverse the magnetic domains reduced from approximately 80 Oe at 0 kV cm^{-1} to approximately 50 Oe at 20 kV cm^{-1}. These results indicate that it is easier to reverse magnetic domains under larger applied electric fields suggesting a decrease in PMA of the Pt/Co/Ta ultrathin films, which is in agreement with the AHE results in Fig. 1a.

As shown in Fig. 1c, a large electric-field modulation of $\frac{R_H}{R_{H,S}}$ was achieved at zero magnetic field. So, we imaged the evolution of the domain structure driven by electric fields without a magnetic field as shown in Fig. S3 (ESI†); meanwhile, Fig. 3 shows the representative images. After saturating the sample with a magnetic field of −200 Oe, almost all the magnetic domains were downward with a white contrast at $E = 0$ kV cm^{-1} (Fig. 3a), which is consistent with the approximate 100% remnant $\frac{R_H}{R_{H,S}}$ in its AHE curve (Fig. 1a). Then, the domain structure did not exhibit any change until an electric field of 10 kV cm^{-1} was applied, at which upward domains were generated, as highlighted by the red circles in Fig. 3c. This generation of upward domains corresponds to the giant modulation of remnant $\frac{R_H}{R_{H,S}}$ between 5 kV cm^{-1} and 10 kV cm^{-1} in Fig. 1c. Further increasing the electric fields did not much affect the domain structures, since the remnant $\frac{R_H}{R_{H,S}}$ slightly changed when the electric fields increased from 10 kV cm^{-1} to 20 kV cm^{-1}. Nevertheless, the electric field induced newly
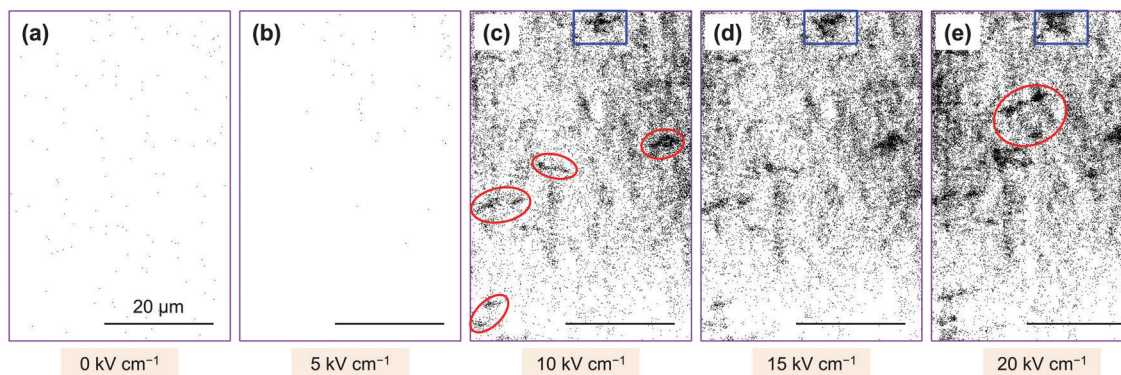
Fig. 3 A dramatic change of the Kerr image was observed between 5 kV cm^{-1} and 10 kV cm^{-1}. The red circles in (c) and (e) highlight newly reversed domains generated by the applied electric field, and the blue square highlights the electric-field-driven domain expansion. Note that the tiny dark spots are caused by noise.

reversed domains, highlighted by the red circle in Fig. 3e, and expanded the magnetic domain shown in the blue square area in Fig. 3c–e. This evolution of domain structures driven by electric fields without a magnetic field agrees with the AHE results in

Fig. 1c and further confirms the giant magnetoelectric effect in the PMN-PT/Pt/Co/Ta multiferroic heterostructure.

The significant modulation of M_Z and the domain structure of the Pt/Co/Ta films by electric fields from the AHE and Kerr
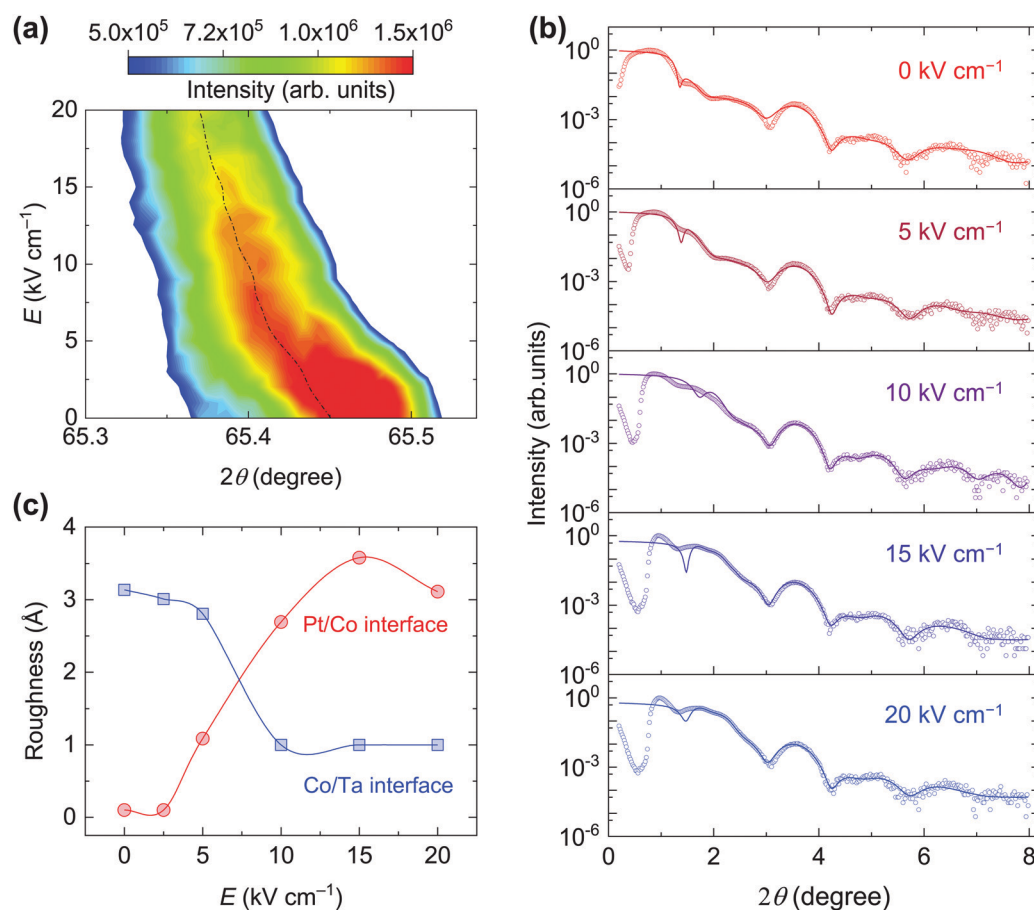
Fig. 4 (a) *In situ* XRD results around the PMN-PT (022) peak with various electric fields. The dashed line shows that the electric field shifted the (022) peak to smaller angles, suggesting a tensile strain generated along the *z* axis as a result of expansion of the out-of-plane lattice. (b) Typical XRR spectra of the Pt/Co/Ta sample with electric fields. The discrepancy of the experimental data and fitting curves at small angles (<1 degree) may result from the variation of electron density induced by the applied electric field, which has a slight effect on fitting the results of the interface roughness. (c) Dependence of Pt/Co and Co/Ta interface roughness on electric field deduced from (b) by fitting XRR spectra. The roughness for both Pt/Co and Co/Ta interfaces changed dramatically between 5 kV cm^{-1} and 10 kV cm^{-1}.

image results revealed a giant magnetoelectric effect. In multiferroic heterostructures, there are two kinds of magnetoelectric couplings mediated by charge and strain,[9] respectively. The 3 nm Ta metal layer inserted between the PMN-PT and Pt/Co/Ta film can eliminate the charge effect because it only affects a few nanometers.[29] Thus, a strain-mediated magnetoelectric coupling should be the main origin of this giant magnetoelectric effect in the PMN-PT/Pt/Co/Ta multiferroic heterostructure. For this type of coupling, the piezostrain of the ferroelectric substrate generated by applying an electric field *via* a converse piezoelectric effect transfers to the magnetic layer, so that the magnetic property of the magnetic layer is modulated through a converse magnetostriction effect, leading to such a magnetoelectric effect.[10] The magnetoelastic anisotropy induced by the piezostrain[16,20,30] is $K_{strain} = \dfrac{3}{2}\varepsilon_z Y\lambda\Big/(1-\nu)$, where λ, Y and ν are the magnetostriction coefficient, Young's modulus, and Poisson ratio of the magnetic layer, respectively. ε_z is the electric-field-induced piezostrain of the ferroelectric substrate along the z-axis and can be estimated by the out-of-plane lattice parameter of the PMN-PT from the XRD measurements.[20] As shown in Fig. 4a, the electric field shifted the (022) diffraction peak of PMN-PT to smaller angles so that the out-of-plane lattice expanded with an increasing electric field, leading to a tensile strain along the z-axis as shown in Fig. S4 (ESI†). Considering the negative magnetostriction coefficient of the Co layer,[14] this tensile strain induced a negative K_{strain}, resulting in a decrease in PMA in the Pt/Co/Ta ultrathin films under electric fields, which qualitatively explains the aforementioned AHE and Kerr results.

Although strain-mediated magnetoelectric coupling has been investigated for a long time, its microscopic mechanism still remains unclear.[9] The PMA of perpendicularly magnetized Pt/Co/Ta ultrathin films originates form interfacial anisotropy, which depends strongly on the interface roughness.[23,24,31] We anticipate that this electrical modulation of PMA in the Pt/Co/Ta film results from an electric field-induced variation in the Pt/Co/Ta interface roughness, which is not considered in previous literature reports.[14–17,19,21,22] To confirm this, we measured *in situ* XRR, a technique that is very sensitive to surface and interface roughness, under electric fields to investigate variations in the Pt/Co/Ta interface roughness. Fig. 4b shows the typical XRR spectra of the Pt/Co/Ta sample under electric fields, and we fitted the XRR data using GenX[32] to obtain the interface roughness. Fig. S5 (ESI†) shows that the roughness of the PMN-PT substrate was approximately 5 Å for an electric field smaller than 5 kV cm⁻¹. Surprisingly, it reached more than 35 Å when the electric field was larger than 15 kV cm⁻¹, and thus the electric field induced a large roughness variation in the PMN-PT substrate. The dependence of the Pt/Co and Co/Ta interface roughness on the electric field is presented in Fig. 4c, in which the electric field increased the roughness of the Pt/Co interface and decreased the roughness of the Co/Ta interface. The reason for this different changing trend of the Pt/Co and Co/Ta interface roughness is unclear now and may be caused by their different bonding energies.[23]

It should be noted that both the Pt/Co and Co/Ta interface roughness exhibited a dramatic change between 5 kV cm⁻¹ and 10 kV cm⁻¹, while $\dfrac{R_H}{R_{H,S}}$ (Fig. 1c) and the magnetic domain (Fig. 3) also exhibited a dramatic change in the same electric field range. This surprising coincidence reveals that the dramatic changes in AHE and the magnetic domain are closely related to the electric field-induced interface roughening, which decreases the interface anisotropy.[23,24,31] It is also notable that inserting a 3 nm Ta thin layer largely suppressed this large substrate roughness variation as shown in Fig. S5 (ESI†). Thus, a thick buffer layer between the PMN-PT substrate and the perpendicularly magnetized layer could further suppress the interface roughness caused by the electric field-induced substrate roughness variation. This could be a reason for the small magnetoelectric effect in the Co/Pt multilayers.[14] Moreover, in Co/Pt multilayers, there are several interfaces contributing to the interface PMA, while our Pt/Co/Ta sample has only two interfaces: Pt/Co and Co/Ta. Thus, the PMA of Pt/Co/Ta is sensitive to interface roughness variations, and it is easy for the electric field-varied substrate roughness to affect the interface PMA *via* interface roughening.

Conclusions

We have demonstrated a giant magnetoelectric effect in the PMN-PT/Pt/Co/Ta multiferroic heterostructure. By applying electric fields to PMN-PT, we observed a remarkable modulation of M_Z at a zero magnetic field, as revealed by the AHE curves and a dramatic change in the magnetic domain structures in the Pt/Co/Ta ultrathin films, as shown by Kerr imaging. This giant magnetoelectric effect results from strain-mediated magnetoelectric coupling, in which an electric field-induced variation in interface roughening plays a vital role. Our results are important for the electrical control of perpendicular magnetization. Moreover, integrating multiferroic and spintronics is considered a promising way to realize energy-efficient spintronic devices, and manipulating in-plane magnetic tunnel junctions using electric fields has been recently reported.[33–35] However, research on the electric field manipulation of perpendicular magnetic tunnel junctions *via* magnetoelectric coupling, which represents a significant step towards energy-efficient spintronic devices, such as magneto-resistive random access memory, is still lacking and urgently required. Therefore, we expect that this giant magnetoelectric effect in perpendicularly magnetized Pt/Co/Ta ultrathin films will promote more research on the electrical manipulation of perpendicular magnetic tunnel junctions.

Experimental section

Sample fabrication

Pt/Co/Ta ultrathin films consisting of Ta (3 nm)/Pt (3 nm)/Co (*t* nm)/Ta (2 nm) multilayers with different Co thicknesses were deposited on PMN-PT (011) substrates (5 mm × 3 mm × 0.2 mm) at room temperature by a Singulus ROTARIS

sputtering system with a base pressure better than 10^{-6} Pa. To apply the electric fields, 10 nm Ti and 150 nm Au films were deposited on the bottom of PMN-PT as an electrode, and a Keithley 6517 electrometer was used. A Kerr microscope in polar geometry was used to image the magnetic domain of the Pt/Co/Ta ultrathin films. The *in situ* XRD and XRR were performed under electric fields using a Rigaku SmartLab 9 kW X-ray diffractometer with Cu Kα radiation. All measurements were carried out at room temperature.

AHE measurements and the determination of the converse magnetoelectric coefficient

The AHE curves were acquired using an electromagnet system with a Keithley 6221 current source and a Keithley 2182 nanovolt meter. The Hall resistance is[17]

$$R_H = R_0 H_Z + R_{AHE} M_Z \tag{1}$$

where the first term represents the ordinary Hall effect, which is proportional to H_Z with a coefficient of R_0. The second term, arising from AHE, is proportional to M_Z, and R_{AHE} is the AHE coefficient. The ordinary Hall component is usually much smaller than the AHE component so the eqn (1) can be rewritten as

$$R_H = R_{AHE} M_Z \tag{2}$$

From eqn (2), the normalized Hall resistance can be found as

$$\frac{R_H}{R_{H,S}} = \frac{M_Z}{M_S} \tag{3}$$

Here, M_S is the saturated magnetization, and $R_{H,S}$ is the Hall resistance measured at M_S under high H_Z.

The converse magnetoelectric coefficient α is given by[9,28]

$$\alpha = \mu_0 \frac{dM_Z}{dE} \tag{4}$$

Using eqn (3) and (4), the converse magnetoelectric coefficient can be deduced from

$$\alpha = \mu_0 \frac{dM_Z}{dE} = \mu_0 M_S \frac{d(R_H/R_{H,S})}{dE} \tag{5}$$

Using eqn (5), α was determined from Fig. 2c, where M_S = 1400 emu cm^{-3} was obtained from the magnetic hysteresis loop measured using MPMS-VSM (Quantum Design).

Author contributions

A. C. conceived the idea and designed the experiments, and X.-X. Z. supervised the project. A. C. performed the magnetic and magnetotransport measurements. H. H., W. L. and Y. L. conducted the XRD and XRR measurements. Y. W. deposited multilayers. S. Z. and A. C. measured Kerr imaging with the help of J. K., and Y. W. extracted the values of the magnetic domain reversal ratio using Mathematics. W. S. and Y. Z. performed the FMR measurements. A. C. and X.-X. Z. analyzed the data and wrote the manuscript. All authors read and commented on the manuscript.

Conflicts of interest

There are no conflicts to declare.

Acknowledgements

References

1 D. Sander, S. O. Valenzuela, D. Makarov, C. H. Marrows, E. E. Fullerton, P. Fischer, J. McCord, P. Vavassori, S. Mangin, P. Pirro, B. Hillebrands, A. D. Kent, T. Jungwirth, O. Gutfleisch, C. G. Kim and A. Berger, *J. Phys. D: Appl. Phys.*, 2017, **50**, 363001.

2 S. Ikeda, K. Miura, H. Yamamoto, K. Mizunuma, H. D. Gan, M. Endo, S. Kanai, J. Hayakawa, F. Matsukura and H. Ohno, *Nat. Mater.*, 2010, **9**, 721–724.

3 L. Liu, C. F. Pai, Y. Li, H. W. Tseng, D. C. Ralph and R. A. Buhrman, *Science*, 2012, **336**, 555–558.

4 M. Wang, W. Cai, D. Zhu, Z. Wang, J. Kan, Z. Zhao, K. Cao, Z. Wang, Y. Zhang, T. Zhang, C. Park, J.-P. Wang, A. Fert and W. Zhao, *Nat. Electron.*, 2018, **1**, 582–588.

5 N. Sato, F. Xue, R. M. White, C. Bi and S. X. Wang, *Nat. Electron.*, 2018, **1**, 508–511.

6 A. J. Tan, M. Huang, C. O. Avci, F. Buttner, M. Mann, W. Hu, C. Mazzoli, S. Wilkins, H. L. Tuller and G. S. D. Beach, *Nat. Mater.*, 2019, **18**, 35–41.

7 C. Bi, Y. Liu, T. Newhouse-Illige, M. Xu, M. Rosales, J. W. Freeland, O. Mryasov, S. Zhang, S. G. te Velthuis and W. G. Wang, *Phys. Rev. Lett.*, 2014, **113**, 267202.

8 F. Matsukura, Y. Tokura and H. Ohno, *Nat. Nanotechnol.*, 2015, **10**, 209–220.

9 J. M. Hu, L. Q. Chen and C. W. Nan, *Adv. Mater.*, 2016, **28**, 15–39.

10 A. T. Chen and Y. G. Zhao, *APL Mater.*, 2016, **4**, 032303.

11 C. A. Vaz, *J. Phys.: Condens. Matter*, 2012, **24**, 333201.

12 T. Taniyama, *J. Phys.: Condens. Matter*, 2015, **27**, 504001.

13 N. X. Sun and G. Srinivasan, *Spin*, 2012, **02**, 1240004.

14 Y. Sun, Y. Ba, A. Chen, W. He, W. Wang, X. Zheng, L. Zou, Y. Zhang, Q. Yang, L. Yan, C. Feng, Q. Zhang, J. Cai, W. Wu, M. Liu, L. Gu, Z. Cheng, C. W. Nan, Z. Qiu, Y. Wu, J. Li and Y. Zhao, *ACS Appl. Mater. Interfaces*, 2017, **9**, 10855–10864.

15 B. Peng, Z. Zhou, T. Nan, G. Dong, M. Feng, Q. Yang, X. Wang, S. Zhao, D. Xian, Z. D. Jiang, W. Ren, Z. G. Ye, N. X. Sun and M. Liu, *ACS Nano*, 2017, **11**, 4337–4345.

16 G. Yu, Z. Wang, M. Abolfath-Beygi, C. He, X. Li, K. L. Wong, P. Nordeen, H. Wu, G. P. Carman, X. Han, I. A. Alhomoudi,

P. K. Amiri and K. L. Wang, *Appl. Phys. Lett.*, 2015, **106**, 072402.

17 P. M. Shepley, A. W. Rushforth, M. Wang, G. Burnell and T. A. Moore, *Sci. Rep.*, 2015, **5**, 7921.

18 M. Ghidini, F. Maccherozzi, X. Moya, L. C. Phillips, W. Yan, J. Soussi, N. Metallier, M. E. Vickers, N. J. Steinke, R. Mansell, C. H. Barnes, S. S. Dhesi and N. D. Mathur, *Adv. Mater.*, 2015, **27**, 1460–1465.

19 Y. Shirahata, R. Shiina, D. L. González, K. J. A. Franke, E. Wada, M. Itoh, N. A. Pertsev, S. van Dijken and T. Taniyama, *NPG Asia Mater.*, 2015, **7**, e198.

20 A. Chen, S. Zhang, Y. Wen, H. Huang, J. Kosel, Y. Lu and X. X. Zhang, *ACS Appl. Mater. Interfaces*, 2019, **11**, 47091–47097.

21 Q. Yang, T. X. Nan, Y. J. Zhang, Z. Y. Zhou, B. Peng, W. Ren, Z. G. Ye, N. X. Sun and M. Liu, *Phys. Rev. Appl.*, 2017, **8**, 044006.

22 D. B. Gopman, C. L. Dennis, P. J. Chen, Y. L. Iunin, P. Finkel, M. Staruch and R. D. Shull, *Sci. Rep.*, 2016, **6**, 27774.

23 J. Yun, Y. Zuo, J. Mao, M. Chang, S. Zhang, J. Liu and L. Xi, *Appl. Phys. Lett.*, 2019, **115**, 032404.

24 T. Devolder, *Phys. Rev. B: Condens. Matter Mater. Phys.*, 2000, **62**, 5794–5802.

25 K. A. Avchaciov, W. Ren, F. Djurabekova, K. Nordlund, I. Sveklo and A. Maziewski, *Phys. Rev. B: Condens. Matter Mater. Phys.*, 2015, **92**, 104109.

26 G. Vinai, F. Motti, V. Bonanni, A. Y. Petrov, S. Benedetti, C. Rinaldi, M. Stella, D. Cassese, S. Prato, M. Cantoni, G. Rossi, G. Panaccione and P. Torelli, *Adv. Electron. Mater.*, 2019, **5**, 1900150.

27 C. Song, B. Cui, F. Li, X. Zhou and F. Pan, *Prog. Mater. Sci.*, 2017, **87**, 33–82.

28 J. M. Hu, C. G. Duan, C. W. Nan and L. Q. Chen, *npj Comput. Mater.*, 2017, **3**, 18.

29 T. Nan, Z. Zhou, M. Liu, X. Yang, Y. Gao, B. A. Assaf, H. Lin, S. Velu, X. Wang, H. Luo, J. Chen, S. Akhtar, E. Hu, R. Rajiv, K. Krishnan, S. Sreedhar, D. Heiman, B. M. Howe, G. J. Brown and N. X. Sun, *Sci. Rep.*, 2014, **4**, 3688.

30 N. Lei, S. Park, P. Lecoeur, D. Ravelosona, C. Chappert, O. Stelmakhovych and V. Holy, *Phys. Rev. B: Condens. Matter Mater. Phys.*, 2011, **84**, 012404.

31 P. Bruno and J. P. Renard, *Appl. Phys. A: Mater. Sci. Process.*, 1989, **49**, 499–506.

32 M. Björck and G. Andersson, *J. Appl. Crystallogr.*, 2007, **40**, 1174–1178.

33 A. Chen, Y. Zhao, Y. Wen, L. Pan, P. Li and X. X. Zhang, *Sci. Adv.*, 2019, **5**, eaay5141.

34 A. Chen, Y. Wen, B. Fang, Y. Zhao, Q. Zhang, Y. Chang, P. Li, H. Wu, H. Huang, Y. Lu, Z. Zeng, J. Cai, X. Han, T. Wu, X. X. Zhang and Y. Zhao, *Nat. Commun.*, 2019, **10**, 243.

35 P. Li, A. Chen, D. Li, Y. Zhao, S. Zhang, L. Yang, Y. Liu, M. Zhu, H. Zhang and X. Han, *Adv. Mater.*, 2014, **26**, 4320–4325.